Hyperon halo structure of C and B isotopes

Ying Zhang [1,2,*] Hiroyuki Sagawa,[2,3,†] and Emiko Hiyama[4,2,‡]
[1]*Department of Physics, School of Science, Tianjin University, Tianjin, 300354, China*
[2]*RIKEN Nishina Center, Wako, Saitama 351-0198, Japan*
[3]*Center for Mathematics and Physics, the University of Aizu, Aizu-Wakamatsu, Fukushima 965-8580, Japan*
[4]*Department of Physics, Tohoku University, 980-8578, Japan*

(Received 17 September 2020; revised 22 February 2021; accepted 9 March 2021; published 25 March 2021)

We study the Λ hypernuclei of C and B isotopes by the Hartree-Fock model with Skyrme-type nucleon-nucleon and Λ-nucleon interactions. The calculated Λ binding energies agree well with the available experiment data. We found halo structure in the Λ $1p$ state with extended wave functions beyond the nuclear surface in the light C and B isotopes. We also found the enhanced electric-dipole transition between Λ $1p$ and $1s$ states, which could be the evidence for this hyperon halo structure.

DOI: 10.1103/PhysRevC.103.034321

I. INTRODUCTION

Since the halo structure of ^{11}Li was observed in 1985 [1], halo phenomena have been studied intensively from both the experimental and theoretical sides [2–5] in the nuclei near and beyond the neutron and also proton drip lines. The halo nuclei are characterized by its extended density profile far beyond the nuclear surface region. Very much enhanced electric-dipole transitions have been also observed in several halo nuclei as a unique phenomenon associated with the extended halo wave function [6]. As a theoretical model, for lighter nuclei such as ^{6}He and ^{11}Li, the framework of core $+ n + n$ three-body model has been adopted often to describe the so-called "Borromean system," in which one-nucleon + core systems have never been bound, but only two-nucleon + core systems make a bound nucleus [7,8].

For *sd*-shell neutron-rich nuclei such as Ne isotopes, some halo states have been found [9]. In addition, deformed structures with larger β_2 have been observed in these systems [10]. In the nuclei so far discussed, one or two nucleons will contribute to create the halo structure. When one goes to heavier nuclei, for instance, in neutron-rich Ca and Zr isotopes, theoretically in Refs. [11–16], a giant halo phenomenon is predicted, in which several neutrons contribute to make halo nuclei.

Let us consider hypernuclei consisting of nuclei and a hyperon, especially a Λ particle. So far, there have been many investigations on the effect of the hyperon in neutron-rich hypernuclei [17–22], and even the explorations of the hyperon halo or hyperon drip line [23,24]. Some authors pointed out that there was the possibility to have halo states in lighter systems [25,26]: In $^3_\Lambda$H, the observed binding energy is 0.13 MeV with respect to the deuteron + Λ threshold, which is a very weakly bound state, and then this system has a Λ halo structure with respect to the deuteron [25]. One of the present authors (E.H.) pointed out that neutron or proton densities in the ground state of $^6_\Lambda$He and excited states of $^7_\Lambda$He and $^7_\Lambda$Li with isospin $T = 1$ have been enhanced within the framework of the $^5_\Lambda$He $+N + N$ three-body model [26]. Thus, the study of halo structure in Λ hypernuclei has been focused on lighter hypernuclei with $A \leqslant 7$. In this paper, we focus on the possibility to have a halo structure in heavier Λ hypernuclei such as boron or carbon isotopes with $A \geqslant 8$. Especially in $^{13}_\Lambda$C we have observed data of the ground state, $1/2^+_1$, and either the $3/2^+_1$ or $5/2^+_1$ positive-parity excited states, and the $3/2^-$ and $1/2^-$ negative-parity excited states. The dominate component of the two negative-parity states is the ^{12}C $\otimes \Lambda(1p)$ configuration. They are important to extract information on the ΛN spin-orbit force: they measured the spin-orbit splitting energy of $1/2^-$-$3/2^-$ to be 0.152 MeV [27,28]. Furthermore, these states are weakly bound by about 1 MeV with respect to the ^{12}C + Λ threshold. This means that we have a chance to find the Λ halo structure in C isotopes. Therefore, in this paper, we focus on these possible Λ halo states. In addition, experimentally, a long isotope chain from ^{8}C to ^{22}C was observed. Considering this situation, we study systematically the ground states and the excited states [C $\otimes \Lambda(1p)$] of C hypernuclei with the Hartree-Fock model using Skyrme-type nucleon-nucleon (NN) and Λ-nucleon (ΛN) interactions. We also discuss the halo structure of hypernuclei and the possibility to observe these halo structures by calculating the reduced transition probability $B(E1)$ from the $\Lambda(1p)$ state to the ground state $\Lambda(1s)$.

For this calculation, we use the Skyrme-Hartree-Fock model [29], which is commonly adopted for the description of the gross properties of the nuclei in a broad region of the mass table. The original Skyrme model has no strangeness degrees of freedom. In 1981, Rayet introduced the Skyrme-type ΛN interaction to describe the hypernuclei within the Skyrme model [30]. Since then, many Skyrme-type ΛN interactions were proposed based on realistic hyperon-nucleon

*yzhangjcnp@tju.edu.cn
†sagawa@ribf.riken.jp
‡hiyama@riken.jp

interactions, stimulated by many hypernuclear data [31–38]. With these interactions, the hypernuclear structures have been investigated extensively [19,39–41]. But most of these investigations did not include the ΛN spin-orbit interaction, since it was expected to be rather small. In this paper, we adopt the Skyrme-type ΛN interaction [34] obtained by the G-matrix calculation from the one-boson-exchange potential with a reduced ΛN spin-orbit coupling strength which can reproduce the spin-orbit splitting of the $1p$ states in ${}^{13}_{\Lambda}$C [27]. The method is also applied to the neighboring boron isotopes to discuss the p-wave Λ hyperon halo structure there. These studies are performed for the first time with this framework.

Organization of the present paper is as follows: In Sec. II, the method is explained. The results are discussed in Sec. III, and we summarize in Sec. IV.

II. THEORETICAL FRAMEWORK

Hypernuclei of C and B isotopes are studied by using HF model with Skyrme-type NN and ΛN interactions. The model is extended to describe systematically from light to heavy hypernuclei including the hyperon degree of freedom. In the Skyrme model, the two-body NN interaction [42] reads

$$\begin{aligned} v_{NN}(\mathbf{r}_1-\mathbf{r}_2) &= t_0(1+x_0P_\sigma)\delta(\mathbf{r}_1-\mathbf{r}_2)+\tfrac{1}{2}t_1(1+x_1P_\sigma)[\boldsymbol{k}'^2\delta(\mathbf{r}_1-\mathbf{r}_2)+\delta(\mathbf{r}_1-\mathbf{r}_2)\boldsymbol{k}^2] \\ &\quad +t_2(1+x_2P_\sigma)\boldsymbol{k}'\cdot\delta(\mathbf{r}_1-\mathbf{r}_2)\boldsymbol{k}+iW_0(\boldsymbol{\sigma}_1+\boldsymbol{\sigma}_2)\cdot\boldsymbol{k}'\delta(\mathbf{r}_1-\mathbf{r}_2)\times\boldsymbol{k}, \end{aligned} \tag{1}$$

where $\boldsymbol{k}=(\overrightarrow{\boldsymbol{\nabla}}_1-\overrightarrow{\boldsymbol{\nabla}}_2)/2i$ is the relative momentum operator acting on the wave functions on the right and $\boldsymbol{k}'=-(\overleftarrow{\boldsymbol{\nabla}}_1-\overleftarrow{\boldsymbol{\nabla}}_2)/2i$ acting on the left, and $P_\sigma=(1+\boldsymbol{\sigma}_1\cdot\boldsymbol{\sigma}_2)/2$ is the spin-exchange operator. The effective density-dependent NN interaction is also introduced as

$$v_{\mathrm{den}-NN}(\mathbf{r}_1,\mathbf{r}_2,\mathbf{r}_3)=\frac{1}{6}t_3(1+x_3P_\sigma)\delta(\mathbf{r}_1-\mathbf{r}_2)\rho^\alpha\Big(\frac{\mathbf{r}_1+\mathbf{r}_2}{2}\Big), \tag{2}$$

where α is the power of density dependence. The Skyrme-type three-body force is equivalent to the interaction (2) with choices of $x_3=1$ and $\alpha=1$ for HF calculations.

The Skyrme-like two-body ΛN interaction is taken as [34]

$$\begin{aligned} v_{\Lambda N}(\mathbf{r}_\Lambda-\mathbf{r}_N) &= t_0^\Lambda\big(1+x_0^\Lambda P_\sigma\big)\delta(\mathbf{r}_\Lambda-\mathbf{r}_N)+\tfrac{1}{2}t_1^\Lambda[\boldsymbol{k}'^2\delta(\mathbf{r}_\Lambda-\mathbf{r}_N)+\delta(\mathbf{r}_\Lambda-\mathbf{r}_N)\boldsymbol{k}^2] \\ &\quad +t_2^\Lambda\boldsymbol{k}'\delta(\mathbf{r}_\Lambda-\mathbf{r}_N)\cdot\boldsymbol{k}+iW_0^\Lambda\boldsymbol{k}'\delta(\mathbf{r}_\Lambda-\mathbf{r}_N)\cdot(\boldsymbol{\sigma}_N+\boldsymbol{\sigma}_\Lambda)\times\boldsymbol{k}, \end{aligned} \tag{3}$$

with an effective density-dependent ΛN force

$$v_{\mathrm{den}-\Lambda N}(\mathbf{r}_\Lambda,\mathbf{r}_N,\rho)=\frac{3}{8}t_3^\Lambda\big(1+x_3^\Lambda P_\sigma\big)\delta(\mathbf{r}_\Lambda-\mathbf{r}_N)\rho^\gamma\Big(\frac{\mathbf{r}_\Lambda+\mathbf{r}_N}{2}\Big), \tag{4}$$

where γ is the power of density dependence.

The total-energy functional can be separated into two parts,

$$E=\int d\mathbf{r}(\mathcal{H}_N+\mathcal{H}_\Lambda), \tag{5}$$

where $\mathcal{H}_N$ is the Hamiltonian density only related with the nucleons, and $\mathcal{H}_\Lambda$ is the one with Λ hyperon degree of freedom. The nucleon Hamiltonian density $\mathcal{H}_N$ can be written as

$$\begin{aligned} \mathcal{H}_N &= \frac{\hbar^2}{2m_N}\tau_N+\frac{1}{2}t_0\Big(1+\frac{1}{2}x_0\Big)\rho_N^2-\frac{1}{2}t_0\Big(x_0+\frac{1}{2}\Big)\big(\rho_n^2+\rho_p^2\big) \\ &\quad +\frac{1}{4}\Big[t_1\Big(1+\frac{1}{2}x_1\Big)+t_2\Big(1+\frac{1}{2}x_2\Big)\Big]\rho_N\tau_N+\frac{1}{4}\Big[-t_1\Big(\frac{1}{2}+x_1\Big)+t_2\Big(\frac{1}{2}+x_2\Big)\Big](\rho_n\tau_n+\rho_p\tau_p) \\ &\quad +\frac{1}{16}\Big[3t_1\Big(1+\frac{1}{2}x_1\Big)-t_2\Big(1+\frac{1}{2}x_2\Big)\Big](\boldsymbol{\nabla}\rho_N)^2 \\ &\quad -\frac{1}{16}\Big[3t_1\Big(\frac{1}{2}+x_1\Big)+t_2\Big(\frac{1}{2}+x_2\Big)\Big][(\boldsymbol{\nabla}\rho_n)^2+(\boldsymbol{\nabla}\rho_p)^2] \\ &\quad +\frac{1}{16}\big[(t_1-t_2)\big(\boldsymbol{J}_n^2+\boldsymbol{J}_p^2\big)-(t_1x_1+t_2x_2)\boldsymbol{J}_N^2\big] \\ &\quad +\frac{1}{12}t_3\Big(1+\frac{1}{2}x_3\Big)\rho_N^{\alpha+2}-\frac{1}{12}t_3\Big(\frac{1}{2}+x_3\Big)\rho_N^\alpha\big(\rho_n^2+\rho_p^2\big) \\ &\quad +\frac{1}{2}W_0(\boldsymbol{\nabla}\rho_N\cdot\boldsymbol{J}_N+\boldsymbol{\nabla}\rho_n\cdot\boldsymbol{J}_n+\boldsymbol{\nabla}\rho_p\cdot\boldsymbol{J}_p)+\mathcal{H}_{\mathrm{Coul.}}. \end{aligned} \tag{6}$$

In Eq. (6) and the following, we define the baryon density ($B = n, p, \Lambda$)

$$\rho_B(\mathbf{r}) = \sum_{i,\sigma} n_i |\phi_{i,B}(\mathbf{r}, \sigma)|^2, \tag{7}$$

the kinetic-energy density

$$\tau_B(\mathbf{r}) = \sum_{i,\sigma} n_i |\nabla\phi_{i,B}(\mathbf{r}, \sigma)|^2, \tag{8}$$

and the spin density

$$\boldsymbol{J}_B(\mathbf{r}) = -i \sum_{i,\sigma,\sigma'} n_i \phi^*_{i,B}(\mathbf{r}, \sigma)[\nabla \times \boldsymbol{\sigma}\phi_{i,B}(\mathbf{r}, \sigma')], \tag{9}$$

where $\phi_{i,B}(\mathbf{r}, \sigma)$ is the wave function of the single-particle state, and n_i is the corresponding occupation number, which is defined by $n_i = v_i^2(2j+1)$. The occupation probability v_i^2 of the single-particle state i will be determined by either BCS or the filling approximation depending on the model. In Eq. (6), the nucleon total densities are defined as $\rho_N = \rho_n + \rho_p$, $\tau_N = \tau_n + \tau_p$, and $\boldsymbol{J}_N = \boldsymbol{J}_n + \boldsymbol{J}_p$.

The Hamiltonian density related with Λ can be written as [37]

$$\begin{aligned}\mathcal{H}_\Lambda = {} & \frac{\hbar^2}{2m_\Lambda}\tau_\Lambda + t_0^\Lambda\left(1+\frac{1}{2}x_0^\Lambda\right)\rho_\Lambda\rho_N + \frac{1}{4}\left(t_1^\Lambda + t_2^\Lambda\right)(\tau_\Lambda\rho_N + \tau_N\rho_\Lambda) \\ & + \frac{1}{8}\left(3t_1^\Lambda - t_2^\Lambda\right)\nabla\rho_\Lambda\cdot\nabla\rho_N + \frac{1}{2}W_0^\Lambda(\nabla\rho_N\cdot\boldsymbol{J}_\Lambda + \nabla\rho_\Lambda\cdot\boldsymbol{J}_N) + \frac{3}{8}t_3^\Lambda\left(1+\frac{1}{2}x_3\right)\rho_N^{\gamma+1}\rho_\Lambda.\end{aligned} \tag{10}$$

As a first step, we assume spherical symmetry for the hypernucleus, and the pairing correlation is not considered explicitly, but the filling approximation is adopted for the occupation probability v_i^2 from the bottom of the potential to the Fermi energy in order. The single-particle wave function for nucleons and Λ can be written as

$$\phi_{i,B}(\mathbf{r}\sigma) = \frac{R_{i,B}(r)}{r} Y_{ljm}(\hat{\mathbf{r}}\sigma), \quad i = (nljm) \text{ and } B = (n, p, \Lambda), \tag{11}$$

where $R_{i,B}(r)$ is the radial wave function, and $Y_{ljm}(\hat{\mathbf{r}}\sigma)$ is the vector spherical harmonics.

To show the model dependence of the calculation, we choose three Skyrme NN interactions SIII [43], SLy4 [44], and SkM* [45], together with different Skyrme-type ΛN interactions such as No. 1 in Ref. [31] (labeled "YBZ1") fit according to the hypernucleus data, No. 1 and No. 5 in Ref. [34] (labeled "LY1" and "LY5") obtained by the G-matrix calculation from the one-boson-exchange potential. In particular, LY5 includes the ΛN spin-orbit interaction with the strength $W_0^\Lambda = 62$ MeV fm^5. However, we found the obtained spin-orbit splitting of the $1p$ states in $^{13}_{\Lambda}$C is too large compared with the experiment data 0.152 MeV [27]. Therefore, we use a reduced value $W_0^\Lambda = 4.7$ MeV fm^5 instead (labeled "LY5r") and obtain a realistic spin-orbit splitting of 0.155 MeV of $1p$ states in $^{13}_{\Lambda}$C calculated with SkM*.

The center-of-mass correction is considered simply by multiplying the factor $1 - m_N/(Am_N + m_\Lambda)$ and $1 - m_\Lambda/(Am_N + m_\Lambda)$ in front of the mass terms $\hbar^2/2m_N$ and $\hbar^2/2m_\Lambda$, respectively. The binding energy of the Λ particle can be calculated by

$$B_\Lambda = B^\Lambda_{A+1} - B_A, \tag{12}$$

where B_A is the total binding energy of the nucleus with A nucleons, and B^Λ_{A+1} is the total binding energy of the hypernucleus with one additional Λ.

III. RESULTS AND DISCUSSIONS

A. Hypernuclei of C isotopes

We first discuss C isotopes since the spin-orbit splitting of hyperon states was observed only in $^{13}_{\Lambda}$C.

Without the Λ hyperon, the total binding energies of $^{8-22}$C calculated with the Skyrme NN interactions SIII, SLy4, and SkM* are shown in Fig. 1(a). The experiment data taken from Ref. [46] are also shown. One can see that the results of SIII and SLy4 are quite consistent with the data, while SkM* provides more binding for the C isotopes with $A \geqq 15$. The deformation effect might play a minor role here. In the present model, the results of all these three NN interactions show that the neutron drip line is ^{22}C.

Adding one Λ hyperon inside the C isotopes, the Λ binding energies of the ground state $1s$ calculated with Skyrme-type ΛN interactions YBZ1, LY1, LY5, and LY5r are shown in Fig. 2(a). The experiment data are taken from Ref. [47] for $^{12}_{\Lambda}$C, and from Ref. [48] for $^{13,14}_{\Lambda}$C. With the NN interaction SIII, ΛN interaction LY1 gives the nice prediction for the Λ binding energy, while YBZ1 leads to a bit less binding and the original LY5 obvious over-binding compared with the available data. With the reduced spin-orbit strength W_0^Λ, LY5r could give quite consistent predictions for the Λ binding energy using different NN interactions, which also agree very well with the available data.

The Λ binding energies of the $1p$ states calculated with the same NN and ΛN interactions are shown in Table I. In YBZ1 and LY1, there is no ΛN spin-orbit interaction. While

TABLE I. Lambda binding energies of the $1p$ states in ${}^{A}_{\Lambda}$C calculated with different NN (SIII, SLy4, SkM*) and ΛN (YBZ1, LY1, LY5, LY5r) effective interactions. The ΛN spin-orbit interaction is included in LY5 and LY5r, where the first and second lines show the binding energies of the $1p_{1/2}$ and $1p_{3/2}$ states, respectively.

Nucleus	SIII + YBZ1	SIII + LY1	SIII + LY5	SIII + LY5r	SLy4 + LY5r	SkM* + LY5r
${}^{12}_{\Lambda}$C	−0.961	−0.521	−1.367	−0.385	−0.329	−0.379
${}^{12}_{\Lambda}$C			0.461	−0.243	−0.194	−0.239
${}^{13}_{\Lambda}$C	−0.305	0.187	−0.758	0.312	0.324	0.273
${}^{13}_{\Lambda}$C			1.226	0.465	0.473	0.428
${}^{14}_{\Lambda}$C	0.439	0.917	−0.041	1.049	1.044	1.010
${}^{14}_{\Lambda}$C			1.912	1.199	1.190	1.160
${}^{15}_{\Lambda}$C	1.155	1.606	0.647	1.741	1.723	1.697
${}^{15}_{\Lambda}$C			2.554	1.888	1.866	1.842
${}^{16}_{\Lambda}$C	1.649	2.095	1.193	2.241	2.207	2.187
${}^{16}_{\Lambda}$C			3.088	2.386	2.348	2.331
${}^{17}_{\Lambda}$C	2.140	2.575	1.731	2.729	2.680	2.666
${}^{17}_{\Lambda}$C			3.608	2.872	2.819	2.809
${}^{18}_{\Lambda}$C	2.627	3.043	2.259	3.204	3.142	3.133
${}^{18}_{\Lambda}$C			4.115	3.345	3.280	3.274
${}^{19}_{\Lambda}$C	3.108	3.501	2.775	3.667	3.594	3.587
${}^{19}_{\Lambda}$C			4.607	3.806	3.730	3.727
${}^{20}_{\Lambda}$C	3.583	3.947	3.278	4.118	4.037	4.028
${}^{20}_{\Lambda}$C			5.086	4.254	4.172	4.167
${}^{21}_{\Lambda}$C	4.051	4.383	3.770	4.556	4.472	4.457
${}^{21}_{\Lambda}$C			5.553	4.691	4.605	4.595
${}^{22}_{\Lambda}$C	4.331	4.643	4.021	4.833	4.736	4.742
${}^{22}_{\Lambda}$C			5.820	4.969	4.869	4.881
${}^{23}_{\Lambda}$C	4.586	4.880	4.250	5.086	4.991	5.000
${}^{23}_{\Lambda}$C			6.066	5.223	5.127	5.140

in LY5 and LY5r, with the ΛN spin-orbit interaction, the first and second lines list the binding energies of the $1p_{1/2}$ and $1p_{3/2}$ states, respectively. One could see that, in ${}^{12}_{\Lambda}$C, most of the $1p$ states are unbound with respect to the ^{11}C+Λ threshold, since their binding energies B_Λ are negative. In ${}^{13}_{\Lambda}$C, most of the results show the weakly bound $1p$ states. With the original spin-orbit strength $W_0^\Lambda = 62$ MeV fm^5, the interactions SIII + LY5 leads to the spin-orbit splitting nearly 2 MeV between the $1p_{1/2}$ and $1p_{3/2}$ states. However, the experiment data [28] show that this splitting is only 0.152 MeV. With the reduced value $W_0^\Lambda = 4.7$ MeV fm^5 in LY5r, different NN interactions SIII, SLy4, and SkM* obtain the consistent $1p$ spin-orbit splittings 0.153, 0.149, and 0.155 MeV, respectively, in ${}^{13}_{\Lambda}$C. Besides, in Ref. [28], the excitation energies of $\Lambda(1p_{1/2})$ and $\Lambda(1p_{3/2})$ states were observed as $E_x = 10.982 \pm 0.031(\text{stat}) \pm 0.056(\text{syst})$ MeV and $E_x = 10.830 \pm 0.031(\text{stat}) \pm 0.056(\text{syst})$ MeV, respectively. The values calculated with SkM* + LY5r are $E_x = 11.344$ and 11.190 MeV for $\Lambda(1p_{1/2})$ and $\Lambda(1p_{3/2})$ states, which show reasonable agreement with the experiment data. With more neutrons, the $1p$ states becomes more deeply bound. But the spin-orbit splittings are almost constant. Moreover, with the same ΛN interaction LY5r, the Λ binding energies and spin-orbit splittings of $1p$ states calculated with different NN interactions are consistent with each other in heavier C hypernuclei.

The above investigations show that the Λ binding energy is mainly determined by the ΛN interaction, almost independent of the NN interaction. In the following, we take the results calculated with the NN interaction SkM* and ΛN interaction LY5r as examples to discuss the possible Λ halo states in C isotopes.

The HF single-particle energies and rms radii of $\Lambda(1s)$ and $\Lambda(1p)$ orbits in C isotopes are listed in Table II. The $\Lambda(1p)$ states in ${}^{12-14}_{\Lambda}$C are quasibound (resonant) or loosely bound states, as shown in Table I. Especially, their rms radii show a peculiar halo nature similar to the halo state in nuclei such as ^{11}Li and ^{11}Be. The wave functions of $\Lambda(1s_{1/2})$ and $\Lambda(1p_{1/2})$ orbits in ${}^{13}_{\Lambda}$C are plotted in Fig. 3(a). The enhancement of rms radii of the $\Lambda(1p)$ orbit is about 60% compared with those of the $\Lambda(1s)$ orbit. Thus we can conclude to find the $\Lambda(1p)$ halo state in ${}^{13}_{\Lambda}$C. For ${}^{12}_{\Lambda}$C and ${}^{14}_{\Lambda}$C hypernuclei, the $\Lambda(1p)$ states also have small binding energies and show a halo structure similar to that of ${}^{13}_{\Lambda}$C.

The matter rms radii $r^{\text{A}}_{\text{rms}}$ of C isotopes are tabulated in Table III. The listed mass radii of C isotopes are observed by heavy-ion reactions [54,55]. The calculated results reproduce

TABLE II. Properties of single-Λ states in hypernucleus ${}^{A}_{\Lambda}$C calculated with the Skyrme NN interaction SkM* and ΛN interaction LY5r: single-particle energy $e_{\rm s.p.}$, the rms radius $r^{\Lambda}_{\rm rms}$ of the corresponding singe-particle state, $B(E1)$ value of the transition from the excited $\Lambda(1p)$ state to the ground $\Lambda(1s)$ state.

Nucleus	$\Lambda(nlj)$	$e_{\rm s.p.}$ (MeV)	$r^{\Lambda}_{\rm rms}$ (fm)	$B(E1)$ (e^2 fm^2)
${}^{9}_{\Lambda}$C	$1s_{1/2}$	−9.478	2.160	
${}^{10}_{\Lambda}$C	$1s_{1/2}$	−10.662	2.141	
${}^{11}_{\Lambda}$C	$1s_{1/2}$	−11.615	2.136	
${}^{12}_{\Lambda}$C	$1s_{1/2}$	−12.433	2.139	
${}^{12}_{\Lambda}$C	$1p_{1/2}$	−1.228	3.679	1.176×10^{-1}
${}^{12}_{\Lambda}$C	$1p_{3/2}$	−1.367	3.604	1.186×10^{-1}
${}^{13}_{\Lambda}$C	$1s_{1/2}$	−13.156	2.144	
${}^{13}_{\Lambda}$C	$1p_{1/2}$	−1.782	3.464	1.030×10^{-1}
${}^{13}_{\Lambda}$C	$1p_{3/2}$	−1.936	3.410	1.036×10^{-1}
${}^{14}_{\Lambda}$C	$1s_{1/2}$	−13.563	2.172	
${}^{14}_{\Lambda}$C	$1p_{1/2}$	−2.357	3.355	9.264×10^{-2}
${}^{14}_{\Lambda}$C	$1p_{3/2}$	−2.506	3.317	9.297×10^{-2}
${}^{15}_{\Lambda}$C	$1s_{1/2}$	−13.941	2.199	
${}^{15}_{\Lambda}$C	$1p_{1/2}$	−2.911	3.287	8.367×10^{-2}
${}^{15}_{\Lambda}$C	$1p_{3/2}$	−3.055	3.259	8.385×10^{-2}
${}^{16}_{\Lambda}$C	$1s_{1/2}$	−14.292	2.218	
${}^{16}_{\Lambda}$C	$1p_{1/2}$	−3.357	3.252	7.524×10^{-2}
${}^{16}_{\Lambda}$C	$1p_{3/2}$	−3.500	3.228	7.537×10^{-2}
${}^{17}_{\Lambda}$C	$1s_{1/2}$	−14.633	2.236	
${}^{17}_{\Lambda}$C	$1p_{1/2}$	−3.792	3.226	6.806×10^{-2}
${}^{17}_{\Lambda}$C	$1p_{3/2}$	−3.935	3.206	6.814×10^{-2}
${}^{18}_{\Lambda}$C	$1s_{1/2}$	−14.962	2.254	
${}^{18}_{\Lambda}$C	$1p_{1/2}$	−4.216	3.207	6.188×10^{-2}
${}^{18}_{\Lambda}$C	$1p_{3/2}$	−4.357	3.189	6.194×10^{-2}
${}^{19}_{\Lambda}$C	$1s_{1/2}$	−15.281	2.270	
${}^{19}_{\Lambda}$C	$1p_{1/2}$	−4.629	3.192	5.653×10^{-2}
${}^{19}_{\Lambda}$C	$1p_{3/2}$	−4.769	3.177	5.657×10^{-2}
${}^{20}_{\Lambda}$C	$1s_{1/2}$	−15.590	2.286	
${}^{20}_{\Lambda}$C	$1p_{1/2}$	−5.031	3.182	5.188×10^{-2}
${}^{20}_{\Lambda}$C	$1p_{3/2}$	−5.170	3.168	5.190×10^{-2}
${}^{21}_{\Lambda}$C	$1s_{1/2}$	−15.890	2.302	
${}^{21}_{\Lambda}$C	$1p_{1/2}$	−5.422	3.174	4.780×10^{-2}
${}^{21}_{\Lambda}$C	$1p_{3/2}$	−5.559	3.162	4.782×10^{-2}
${}^{22}_{\Lambda}$C	$1s_{1/2}$	−16.038	2.315	
${}^{22}_{\Lambda}$C	$1p_{1/2}$	−5.648	3.191	4.405×10^{-2}
${}^{22}_{\Lambda}$C	$1p_{3/2}$	−5.787	3.178	4.407×10^{-2}
${}^{23}_{\Lambda}$C	$1s_{1/2}$	−16.176	2.326	
${}^{23}_{\Lambda}$C	$1p_{1/2}$	−5.853	3.208	4.070×10^{-2}
${}^{23}_{\Lambda}$C	$1p_{3/2}$	−5.992	3.195	4.072×10^{-2}

TABLE III. The calculated mass rms radius $r^{\rm A}_{\rm rms}$ of isotopes ^{A}C, the corresponding experiment data $r^{\rm A}_{\rm rms}$(expt.) taken from Refs. [54,55], and the calculated mass rms radius of the core $r^{\rm coreA}_{\rm rms}$ in hypernucleus ${}^{A+1}_{\Lambda}$C.

Nucleus	$r^{\rm A}_{\rm rms}$ (fm)	$r^{\rm A}_{\rm rms}$(expt.) (fm)	$\Lambda(nlj)$	$r^{\rm coreA}_{\rm rms}$ (fm)
^{8}C	2.5573		$1s_{1/2}$	2.5020
^{9}C	2.4408		$1s_{1/2}$	2.4120
^{10}C	2.4098		$1s_{1/2}$	2.3902
^{11}C	2.4094		$1s_{1/2}$	2.3942
^{11}C			$1p_{1/2}$	2.4169
^{11}C			$1p_{3/2}$	2.4158
^{12}C	2.4228	2.35±0.02	$1s_{1/2}$	2.4103
^{12}C			$1p_{1/2}$	2.4290
^{12}C			$1p_{3/2}$	2.4280
^{13}C	2.5095	2.28± 0.04	$1s_{1/2}$	2.4943
^{13}C			$1p_{1/2}$	2.5125
^{13}C			$1p_{3/2}$	2.5116
^{14}C	2.5860	2.30 ± 0.07	$1s_{1/2}$	2.5690
^{14}C			$1p_{1/2}$	2.5865
^{14}C			$1p_{3/2}$	2.5856
^{15}C	2.6570	2.50 ± 0.08	$1s_{1/2}$	2.6385
^{15}C			$1p_{1/2}$	2.6554
^{15}C			$1p_{3/2}$	2.6545
^{16}C	2.7193	2.70 ± 0.03	$1s_{1/2}$	2.6999
^{16}C			$1p_{1/2}$	2.7160
^{16}C			$1p_{3/2}$	2.7152
^{17}C	2.7747	2.72 ± 0.03	$1s_{1/2}$	2.7545
^{17}C			$1p_{1/2}$	2.7700
^{17}C			$1p_{3/2}$	2.7692
^{18}C	2.8243	2.82 ± 0.04	$1s_{1/2}$	2.8037
^{18}C			$1p_{1/2}$	2.8186
^{18}C			$1p_{3/2}$	2.8179
^{19}C	2.8692	3.13 ± 0.07	$1s_{1/2}$	2.8484
^{19}C			$1p_{1/2}$	2.8628
^{19}C			$1p_{3/2}$	2.8620
^{20}C	2.9102	2.98 ± 0.05	$1s_{1/2}$	2.8894
^{20}C			$1p_{1/2}$	2.9032
^{20}C			$1p_{3/2}$	2.9025
^{21}C	3.0054		$1s_{1/2}$	2.9833
^{21}C			$1p_{1/2}$	2.9952
^{21}C			$1p_{3/2}$	2.9944
^{22}C	3.0995	3.44 ± 0.08	$1s_{1/2}$	3.0762
^{22}C			$1p_{1/2}$	3.0865
^{22}C			$1p_{3/2}$	3.0858

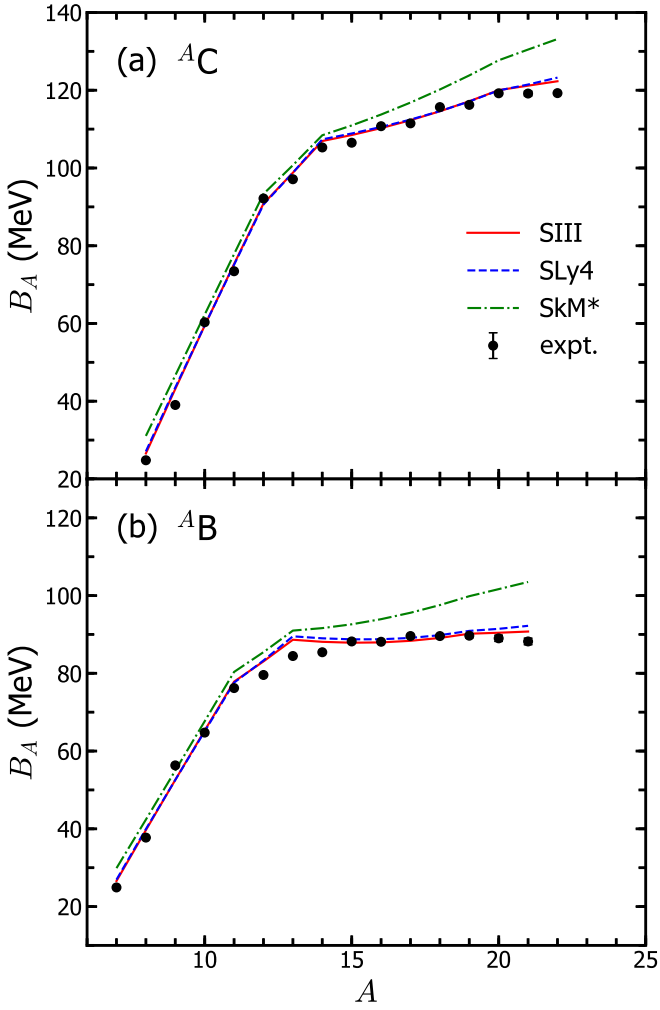

FIG. 1. Total binding energies of (a) carbon and (b) boron isotopes with mass number A calculated with different Skyrme NN interactions: SIII, SLy4, and SkM*. The experiment data [46] are also shown.

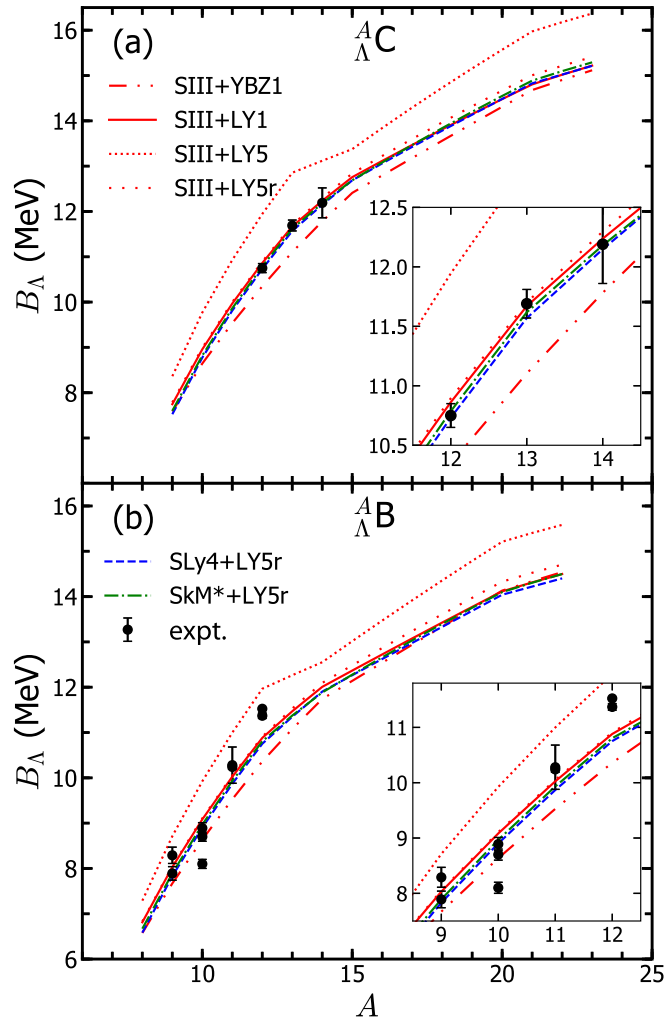

FIG. 2. Lambda binding energy B_Λ of the ground state of hypernucleus (a) $^{A}_{\Lambda}$C and (b) $^{A}_{\Lambda}$B calculated with Skyrme functionals for different NN interactions: SIII, SLy4, and SkM*, and different ΛN interactions: YBZ1, LY1, LY5, and LY5r. The results of SIII + LY1 (solid line) are almost identical to those of SIII + LY5r (loosely dotted line), Sly4 + LY5r (dashed line), and SkM* + LY5r (dash-dotted line), which are enlarged in the insets for $^{12-14}_{\Lambda}$C and $^{9-12}_{\Lambda}$B, respectively. The experiment data [47–53] are also shown.

reasonably well the experiment values except for the neutron halo nuclei ^{19}C and ^{22}C. The rms radii of the cores of corresponding hypernuclei are also listed as $r^{\rm coreA}_{\rm rms}$. In comparison between $r^{\rm A}_{\rm rms}$ and $r^{\rm coreA}_{\rm rms}$, we find a shrinkage or expansion effect of the core nucleus in the hypernucleus. For the $\Lambda(1s)$ hyperon case, we can see a small shrinkage effect of the core, 0.05–0.02 fm, from light to heavy C isotopes. For the $\Lambda(1p)$ hyperon case, it is interesting to see an expansion effect of the core for nuclei $A \leqslant 13$, but quantitatively it is even smaller than the shrinkage effect of the $\Lambda(1s)$ hyperon in the same nucleus.

B. Hypernuclei of B isotopes

The same calculations are also done for the hypernuclei of B isotopes. First, the total binding energies of $^{7-21}$B without hyperons calculated with different Skyrme NN interactions: SIII, SLy4, and SkM* are shown in Fig. 1(b), comparing with the experiment data [46]. Similar with the results of C isotopes, SkM* provides more binding than SLy4 and SIII for $A > 13$. Although the spin-spin interaction is missing in the present Skyrme energy density functional, which might play an important role in odd-even or odd-odd nuclei, most of the present results are consistent with the experiment data except for $^{12-14}$B. Adding one Λ hyperon inside, the Λ binding energies of the ground state $1s$ in the B hypernuclei calculated with different ΛN and NN interactions are shown in Fig. 2(b). The experiment data are taken from Refs. [49–53]. Similar to the C hypernuclei, all the interaction combinations give the consistent Λ binding energies except SIII + LY5, which makes the Λ hyperon over-bind. It is interesting to find that, although the ΛN interaction LY5r is adjusted to the experiment data of $^{13}_{\Lambda}$C, the calculated results for B hypernuclei are also in reasonable agreement with the available experiment data, while there are some uncertainties in the experiment data. The reasonable

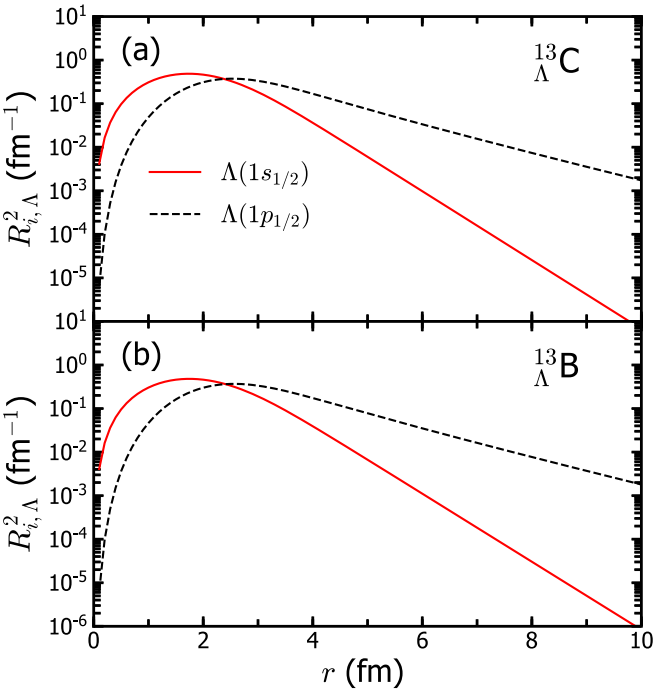

FIG. 3. The square of single-Λ wave function $R^2_{i,\Lambda}$ of $\Lambda(1s_{1/2})$ and $\Lambda(1p_{1/2})$ states in the hypernucleus (a) $^{13}_{\Lambda}$C and (b) $^{13}_{\Lambda}$B, respectively.

agreement between the calculated and experimental results of B_Λ in Figs. 1 and 2 ensures the applicability of the present ΛN interaction to a wide mass region of hypernuclei, at least to most of p-shell hypernuclei.

The Λ single-particle energies, binding energies, and the rms radius of $1s$ and $1p$ states calculated with Skyrme NN interaction SkM* and ΛN interaction LY5r are listed in Table IV. The potential depth is becoming deeper for heavier isotopes and the binding energy of $\Lambda(1s_{1/2})$ state increases from 8.97 MeV in $^{10}_{\Lambda}$B to 14.50 MeV in $^{22}_{\Lambda}$B. The halo structure of $1p$ orbits can be also seen in light B isotopes, especially in $^{12}_{\Lambda}$B and $^{13}_{\Lambda}$B. The wave functions of $\Lambda(1s_{1/2})$ and $\Lambda(1p_{1/2})$ orbits in $^{13}_{\Lambda}$B are drawn in Fig. 3(b). The wave functions in $^{13}_{\Lambda}$B are essentially identical to those of $^{13}_{\Lambda}$C. The spin-orbit splittings in B isotopes show a similar feature to that in C isotopes; $\Delta\varepsilon(\Lambda(1p_{1/2}) - \Lambda(1p_{3/2})) = 0.138$ MeV in $^{13}_{\Lambda}$B and $\Delta\varepsilon(\Lambda(1p_{1/2}) - \Lambda(1p_{3/2})) = 0.129$ MeV for a heavier isotope $^{22}_{\Lambda}$B. Two $\Lambda(1p)$ states were also observed in Ref. [52], as $J^\pi = (1^+_1$ or $2^+_1)$ and $(2^+_2$ or $3^+_1)$ states, which are considered as coupling states of the $3/2^-$ ground state of ^{11}B and $\Lambda(1p_{3/2})$ or $\Lambda(1p_{1/2})$ states. Since the spin-spin interaction of ΛN is not included in the present HF calculations, we cannot predict precisely the energy splitting of 1^+, 2^+, and 3^+ states. However, the HF excitation energies of $\Lambda(1p)$ states $E_x \approx 11.1$ MeV are reasonable compared with the experiment data $E_x(\text{expt.}) = 10.24 \pm 0.05$ and 10.99 ± 0.03 MeV for $J^\pi = (1^+_1$ or $2^+_1)$ and $(2^+_2$ or $3^+_1)$ states, respectively.

TABLE IV. Properties of single-Λ states in hypernucleus $^{A}_{\Lambda}$B calculated with the Skyrme NN interaction SkM* and ΛN interaction LY5r: single-particle energy $e_{\text{s.p.}}$, binding energy B_Λ, rms radius r^{Λ}_{rms} of the corresponding single-particle state, and $B(E1)$ value of the transition from the excited $\Lambda(1p)$ state to the ground $\Lambda(1s)$ state.

Nucleus	$\Lambda(nlj)$	$e_{\text{s.p.}}$ (MeV)	B_Λ (MeV)	r^{Λ}_{rms} (fm)	$B(E1)$ (e^2 fm^2)
$^{8}_{\Lambda}$B	$1s_{1/2}$	−8.750	6.670	2.148	
$^{9}_{\Lambda}$B	$1s_{1/2}$	−9.917	7.892	2.132	
$^{10}_{\Lambda}$B	$1s_{1/2}$	−10.877	8.968	2.128	
$^{11}_{\Lambda}$B	$1s_{1/2}$	−11.712	9.932	2.131	
$^{12}_{\Lambda}$B	$1s_{1/2}$	−12.457	10.805	2.137	
$^{12}_{\Lambda}$B	$1p_{1/2}$	−1.229	−0.386	3.674	8.1524×10^{-2}
$^{12}_{\Lambda}$B	$1p_{3/2}$	−1.370	−0.245	3.599	8.2226×10^{-2}
$^{13}_{\Lambda}$B	$1s_{1/2}$	−12.843	11.375	2.168	
$^{13}_{\Lambda}$B	$1p_{1/2}$	−1.787	0.364	3.503	7.3314×10^{-2}
$^{13}_{\Lambda}$B	$1p_{3/2}$	−1.925	0.502	3.454	7.3684×10^{-2}
$^{14}_{\Lambda}$B	$1s_{1/2}$	−13.205	11.885	2.198	
$^{14}_{\Lambda}$B	$1p_{1/2}$	−2.331	1.061	3.402	6.6020×10^{-2}
$^{14}_{\Lambda}$B	$1p_{3/2}$	−2.465	1.195	3.367	6.6216×10^{-2}
$^{15}_{\Lambda}$B	$1s_{1/2}$	−13.544	12.277	2.218	
$^{15}_{\Lambda}$B	$1p_{1/2}$	−2.765	1.549	3.352	5.9055×10^{-2}
$^{15}_{\Lambda}$B	$1p_{3/2}$	−2.898	1.682	3.323	5.9190×10^{-2}
$^{16}_{\Lambda}$B	$1s_{1/2}$	−13.876	12.660	2.237	
$^{16}_{\Lambda}$B	$1p_{1/2}$	−3.193	2.028	3.315	5.3143×10^{-2}
$^{16}_{\Lambda}$B	$1p_{3/2}$	−3.325	2.160	3.291	5.3233×10^{-2}
$^{17}_{\Lambda}$B	$1s_{1/2}$	−14.203	13.034	2.255	
$^{17}_{\Lambda}$B	$1p_{1/2}$	−3.613	2.497	3.287	4.8090×10^{-2}
$^{17}_{\Lambda}$B	$1p_{3/2}$	−3.744	2.628	3.266	4.8151×10^{-2}
$^{18}_{\Lambda}$B	$1s_{1/2}$	−14.522	13.399	2.273	
$^{18}_{\Lambda}$B	$1p_{1/2}$	−4.026	2.956	3.265	4.3743×10^{-2}
$^{18}_{\Lambda}$B	$1p_{3/2}$	−4.156	3.086	3.247	4.3784×10^{-2}
$^{19}_{\Lambda}$B	$1s_{1/2}$	−14.834	13.754	2.290	
$^{19}_{\Lambda}$B	$1p_{1/2}$	−4.430	3.403	3.249	3.9977×10^{-2}
$^{19}_{\Lambda}$B	$1p_{3/2}$	−4.559	3.532	3.233	4.0005×10^{-2}
$^{20}_{\Lambda}$B	$1s_{1/2}$	−15.138	14.099	2.306	
$^{20}_{\Lambda}$B	$1p_{1/2}$	−4.825	3.839	3.236	3.6695×10^{-2}
$^{20}_{\Lambda}$B	$1p_{3/2}$	−4.952	3.966	3.222	3.6713×10^{-2}
$^{21}_{\Lambda}$B	$1s_{1/2}$	−15.276	14.306	2.319	
$^{21}_{\Lambda}$B	$1p_{1/2}$	−5.034	4.112	3.254	3.3640×10^{-2}
$^{21}_{\Lambda}$B	$1p_{3/2}$	−5.163	4.241	3.239	3.3659×10^{-2}
$^{22}_{\Lambda}$B	$1s_{1/2}$	−15.406	14.497	2.330	
$^{22}_{\Lambda}$B	$1p_{1/2}$	−5.224	4.360	3.271	3.0932×10^{-2}
$^{22}_{\Lambda}$B	$1p_{3/2}$	−5.353	4.489	3.257	3.0952×10^{-2}

C. Eclectic-dipole transition in hypernuclei

We study the electric-dipole transition between hyperon $1p$ and $1s$ state. Electromagnetic transitions may provide precise information of hyperon wave functions in a quantitative manner. Suppose the hypernucleus is initially in the excited state, e.g., Λ is in the $1p$ orbit, it will decay to the ground-state $1s$ orbit. This $E1$ transition has the reduced transition probability

[56]

$$B(E1;J_i \to J_f) = \frac{3e_\Lambda^2}{4\pi}\langle f|r|i\rangle^2(2j_f+1)\begin{pmatrix} j_f & 1 & j_i \\ -\frac{1}{2} & 0 & \frac{1}{2}\end{pmatrix}^2, \tag{13}$$

where e_Λ is the effective charge for Λ hyperon and the integration $\langle f|r|i\rangle$ can be calculated by the radial wave functions of the initial and final single-Λ state as

$$\langle f|r|i\rangle = \int_0^\infty R_{f,\Lambda}(r) r R_{i,\Lambda}(r) dr. \tag{14}$$

Since hyperons Λ have no electric charges, the effective charge in Eq. (13) is given as

$$e_\Lambda^{(E1)} = -ZM_\Lambda e/(AM_N + M_\Lambda), \tag{15}$$

due to the recoil of the core nucleus [57].

The calculated $B(E1)$ values are listed in Tables II for C isotopes and IV for B isotopes. The values are larger in light isotopes than those in heavier nuclei because of the effective charge in Eq. (15). The $B(E1: 1p_{3/2} \to 1s_{1/2}) = 0.1036\ e^2\,\mathrm{fm}^2$ of hyperon configurations in ${}^{13}_{\Lambda}$C corresponds to $0.29B_W(E1)$, where $B_W(E1)$ is the Weisskopf unit (single-particle unit) of the electric-dipole transition in $A = 13$ nucleus. The decay half-life $t_{1/2}$ is estimated as

$$t_{1/2} = \frac{\ln 2}{T(E1)} = 2.99 \times 10^{-18}\ \mathrm{s}, \tag{16}$$

where T is the decay rate,

$$T(E1) = 1.59 \times 10^{15}(E_x)^3 B(E1) = 2.31 \times 10^{17}\ \mathrm{s}^{-1}. \tag{17}$$

The $T(E1)$ is evaluated to be $1.51 \times 10^{17}\ \mathrm{s}^{-1}$ for the transition $\Lambda(1p_{3/2}) \to \Lambda(1s_{1/2})$ in ${}^{13}_{\Lambda}$B and the half-life is estimated to be $t_{1/2} = 4.60 \times 10^{-18}$ s.

In halo nuclei without the Λ degree of freedom, the largest $B(E1)$ transition between discrete states is observed in the $2s_{1/2} \to 1p_{1/2}$ transition in ^{11}Be [58]; $B(E1; 2s_{1/2} \to 1p_{1/2}) = 0.099 \pm 0.010\ \ e^2\,\mathrm{fm}^2 = 0.31 \pm 0.03 B_W(E1)$, which is almost the same strength as $B(E1: \Lambda(1p_{3/2}) \to \Lambda(1s_{1/2}))$ of hyperon configurations in ${}^{13}_{\Lambda}$C. Notice these $B(E1)$ in halo nuclei (hypernuclei) are two to three orders of magnitude larger than normal $B(E1)$, which is less than $10^{-3}\ e^2\,\mathrm{fm}^2$. The $B(E1)$ strength of halo nuclei was studied also by the Coulomb breakup reactions, which measure the excitation from the halo state to the continuum. In these reactions, the $B(E1)$ value was found $B(E1: \mathrm{expt.}) = 1.05 \pm 0.06\ e^2\,\mathrm{fm}^2$ in ^{11}Be [59] and $B(E1: \mathrm{expt.}) = 0.71 \pm 0.07\ e^2\,\mathrm{fm}^2$ in ^{19}C [60]. Systematic measurements of electromagnetic transitions in $\Lambda(1p)$ states may give us a peculiar nuclear structure information including the characteristic features of hyperon halo wave functions.

Here we should mention that the present Skyrme Hartree-Fock model is not suitable for the very weakly bound states. Instead, the Hartree-Fock-Bogoliubov model with pairing correlation and continuum effects [61,62] will be more reliable for these states. However, in the present investigation, we apply the simple Hartree-Fock model as the first step, since the single-particle wave function is straightforward to calculate the transition probability as shown in Eq. (13). The next step to include the pairing and continuum effects is in progress.

IV. SUMMARY AND FUTURE PERSPECTIVES

In this work, we calculated the Λ single-particle states systematically in the C and B isotopes using the HF approach with the Skyrme-type ΛN interaction derived from the G-matrix calculation of the one-boson-exchange potential. We tuned the strength of ΛN spin-orbit interaction by fitting to the observed spin-orbit splitting data of $1/2^-$-$3/2^-$ states in ${}^{13}_{\Lambda}$C. The Λ binding energies thus obtained agree with the available experiment data quite well for the C and B hypernuclei. In the light hypernuclei ${}^{12-14}_{\Lambda}$C and ${}^{12-14}_{\Lambda}$B, we found very weakly bound excited $1p$ orbits for the Λ hyperon, which could have much extended density and large rms radii compared with the ground $1s$ state. Furthermore, we calculated $B(E1)$ values. This halo structure may provide the enhanced $E1$ transition from the excited $1p$ states to the ground $1s$ state, which is a challenging open problem for the future experiment. On the other hand, with more neutrons, the Λ levels become more deeply bound, so that the hyperon halo structure disappears.

ACKNOWLEDGMENTS

This work was supported by JSPS KAKENHI Grants No. JP19K03858 and No. JP18H05407, and the China Scholarship Council (Grant No. 201906255002).

[1] I. Tanihata, H. Hamagaki, O. Hashimoto, Y. Shida, N. Yoshikawa, K. Sugimoto, O. Yamakawa, T. Kobayashi, and N. Takahashi, Phys. Rev. Lett. **55**, 2676 (1985).
[2] A. S. Jensen, K. Riisager, D. V. Fedorov, and E. Garrido, Rev. Mod. Phys. **76**, 215 (2004).
[3] B. Jonson, Phys. Rep. **389**, 1 (2004).
[4] K. Hagino, I. Tanihata, and H. Sagawa, *100 Years of Subatomic Physics* (World Scientific, Singapore, 2013), p. 231.
[5] J. Meng and S. G. Zhou, J. Phys. G **42**, 093101 (2015).
[6] T. Nakamura *et al.*, Phys. Rev. Lett. **96**, 252502 (2006).
[7] M. V. Zhukov *et al.*, Phys. Rep. **231**, 151 (1993).
[8] G. F. Bertsch and H. Esbensen, Ann. Phys. (NY) **209**, 327 (1991).
[9] T. Nakamura *et al.*, Phys. Rev. Lett. **103**, 262501 (2009).
[10] M. Takechi *et al.*, Phys. Lett. B **707**, 357 (2012).
[11] J. Meng and P. Ring, Phys. Rev. Lett. **80**, 460 (1998).
[12] J. Meng, H. Toki, J. Y. Zeng, S. Q. Zhang, and S. G. Zhou, Phys. Rev. C **65**, 041302(R) (2002).
[13] S. Q. Zhang, J. Meng, and S. G. Zhou, Sci. China (Series G) **46**, 632 (2003).
[14] J. Terasaki, S. Q. Zhang, S. G. Zhou, and J. Meng, Phys. Rev. C **74**, 054318 (2006).
[15] M. Grasso, S. Yoshida, N. Sandulescu, and N. Van Giai, Phys. Rev. C **74**, 064317 (2006).
[16] Y. Zhang, M. Matsuo, and J. Meng, Phys. Rev. C **86**, 054318 (2012).

[17] D. Vretenar, W. Pöschl, G. A. Lalazissis, and P. Ring, Phys. Rev. C **57**, R1060(R) (1998).
[18] H. F. Lv, J. Meng, S. Q. Zhang, and S. G. Zhou, Eur. Phys. J. A **17**, 19 (2003).
[19] X. R. Zhou, A. Polls, H. J. Schulze, and I. Vidana, Phys. Rev. C **78**, 054306 (2008).
[20] A. Umeya and T. Harada, Phys. Rev. C **79**, 024315 (2009).
[21] A. Gal and D. J. Millener, Phys. Lett. B **725**, 445 (2013).
[22] R. Wirth and R. Roth, Phys. Lett. B **779**, 336 (2018).
[23] H. F. Lv and J. Meng, Chin. Phys. Lett. **19**, 1775 (2002).
[24] E. Khan, J. Margueron, F. Gulminelli, and A. R. Raduta, Phys. Rev. C **92**, 044313 (2015).
[25] K. Miyagawa, H. Kamada, W. Glöckle, and V. Stoks, Phys. Rev. C **51**, 2905 (1995).
[26] E. Hiyama, M. Kamimura, T. Motoba, T. Yamada, and Y. Yamamoto, Phys. Rev. C **53**, 2075 (1996).
[27] S. Ajimura *et al.*, Phys. Rev. Lett. **86**, 4255 (2001).
[28] H. Kohri *et al.*, Phys. Rev. C **65**, 034607 (2002).
[29] D. Vautherin, Phys. Rev. C **7**, 296 (1973).
[30] M. Rayet, Nucl. Phys. A **367**, 381 (1981).
[31] Y. Yamamoto, H. Bando, and J. Zofka, Prog. Theor. Phys. **80**, 757 (1988).
[32] D. J. Millener, C. B. Dover, and A. Gal, Phys. Rev. C **38**, 2700 (1988).
[33] F. Fernández, T. López-Arias, and C. Prieto, Z. Phys. A - Atomic Nuclei **334**, 349 (1989).
[34] D. E. Lanskoy and Y. Yamamoto, Phys. Rev. C **55**, 2330 (1997).
[35] J. Cugnon, A. Lejeune, and H. J. Schulze, Phys. Rev. C **62**, 064308 (2000).
[36] I. Vidana, A. Polls, A. Ramos, and H. J. Schulze, Phys. Rev. C **64**, 044301 (2001).
[37] N. Guleria, S. K. Dhiman, and R. Shyam, Nucl. Phys. A **886**, 71 (2012).
[38] H. J. Schulze and T. Rijken, Phys. Rev. C **88**, 024322 (2013).
[39] X. R. Zhou, H. J. Schulze, H. Sagawa, C. X. Wu, and E. G. Zhao, Phys. Rev. C **76**, 034312 (2007).
[40] M. T. Win, K. Hagino, and T. Koike, Phys. Rev. C **83**, 014301 (2011).
[41] A. Li, E. Hiyama, X.-R. Zhou, and H. Sagawa, Phys. Rev. C **87**, 014333 (2013).
[42] M. Bender, P.-H. Heenen, and P.-G. Reinhard, Rev. Mod. Phys. **75**, 121 (2003).
[43] M. Beiner, H. Flocard, N. Van Giai, and P. Quentin, Nucl. Phys. A **238**, 29 (1975).
[44] E. Chabanat, P. Bonche, P. Haensel, J. Meyer, and R. Schaeffer, Nucl. Phys. A **635**, 231 (1998).
[45] J. Bartel, P. Quentin, M. Brack, C. Guet, and H.-B. Håkansson, Nucl. Phys. A **386**, 79 (1982).
[46] M. Wang, G. Audi, F. G. Kondev, W. J. Huang, S. Naimi, and X. Xu, Chin. Phys. C **41**, 030003 (2017).
[47] P. H. Pile *et al.*, Phys. Rev. Lett. **66**, 2585 (1991).
[48] T. Cantwell *et al.*, Nucl. Phys. A **236**, 445 (1974).
[49] M. Jurič *et al.*, Nucl. Phys. B **52**, 1 (1973).
[50] T. Hasegawa *et al.*, Phys. Rev. C **53**, 1210 (1996).
[51] D. H. Davis, Nucl. Phys. A **754**, 3c (2005).
[52] L. Tang *et al.*, Phys. Rev. C **90**, 034320 (2014).
[53] E. Botta, T. Bressani, and A. Feliciello, Nucl. Phys. A **960**, 165 (2017).
[54] A. Ozawa *et al.*, Nucl. Phys. A **691**, 599 (2001).
[55] Y. Togano *et al.*, Phys. Lett. B **761**, 412 (2016).
[56] P. Ring, P. Schuck, *The Nuclear Many-Body Problem* (Springer-Verlag, Berlin, Heidelberg, 2004), p. 591, Appendix B.5.
[57] T. Motoba, H. Bando, K. Ikeda, and T. Yamada, Prog. Theor. Phys. Suppl. **81**, 42 (1985).
[58] T. Nakamura *et al.*, Phys. Lett. B **394**, 11 (1997).
[59] N. Fukuda *et al.*, Phys. Rev. C **70**, 054606 (2004).
[60] T. Nakamura *et al.*, Phys. Rev. Lett. **83**, 1112 (1999).
[61] J. Dobaczewski, H. Flocard, and J. Treiner, Nucl. Phys. A **422**, 103 (1984).
[62] J. Meng, H. Toki, S. G. Zhou, S. Q. Zhang, W. H. Long, and L. S. Geng, Prog. Part. Nucl. Phys. **57**, 470 (2006).